Electronic supplementary information

Binding Affinity and Conformation of Conjugated AS1411 Aptamer at Cationic Lipid Bilayer Interface

Penghua Li, Liqun Wang, Meng Sun, Jiyuan Yao, Wenhui Li, Wangting Lu, Youhua Zhou, Geng Zhang, Chenglong Hu, Wanquan Zheng, Feng Wei*

S1. SFG spectra of Au film

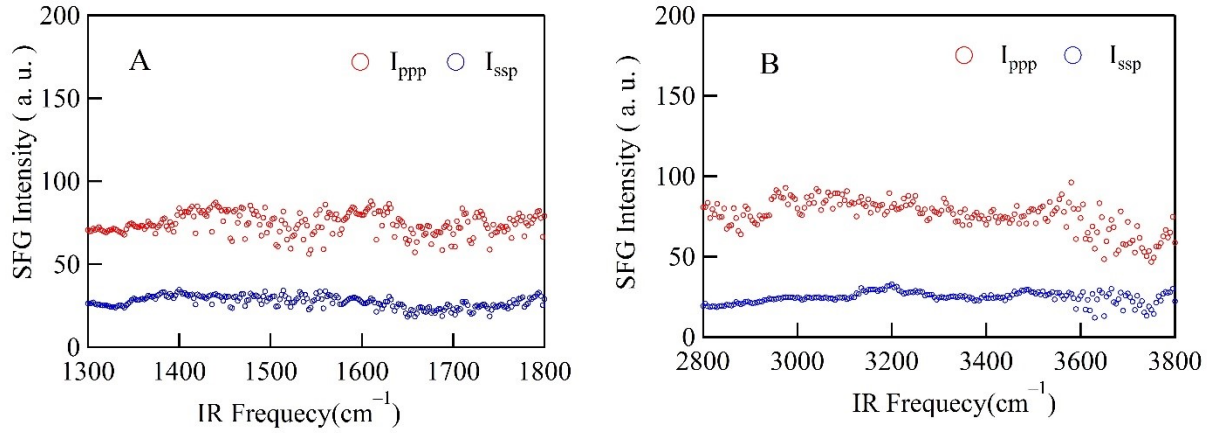

Figure S1 SFG spectra of Au film at the CaF_2 prism interface within the wavenumber ranges of (A) 1300−1800 cm^{-1} and (B) 2800−3800 cm^{-1}.

S2. SFG spectra of deposited monolayers

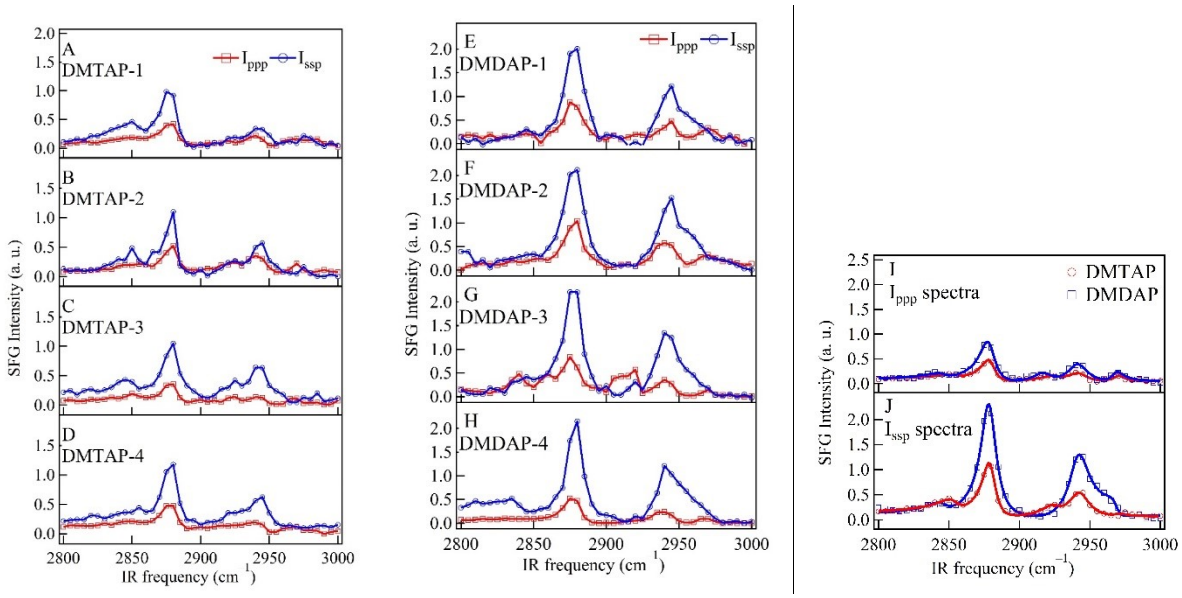

Figure S2 SFG spectra of the deposited (A-D) DMTAP monolayers and (E-H) DMDAP monolayers at the CaF_2/air interface. The averaged (I) I_{ppp} spectra and (J) I_{ssp} spectra of the DMTAP monolayer and DMDAP monolayer.

S3. Zeta potential results of DMTAP and DMDAP liposomes.

For Zeta potential measurements, the lipid vesicles with a diameter of 400 nm were prepared by the vesicle extruder (Avanti polar lipids Inc.). The samples of lipid vesicles were dissolved in DI water with a concentration of 20 μM. Zeta potential measurements were performed on Zetasizer Nano ZS90 (Malvern Instruments) using a U-shaped sample cell via laser Doppler Velocimetry. The sample cell was rinsed with ethanol then DI water at least 3 times before adding the solution of lipid vesicles. The measurements were repeated 3 times for repeatability and accuracy.

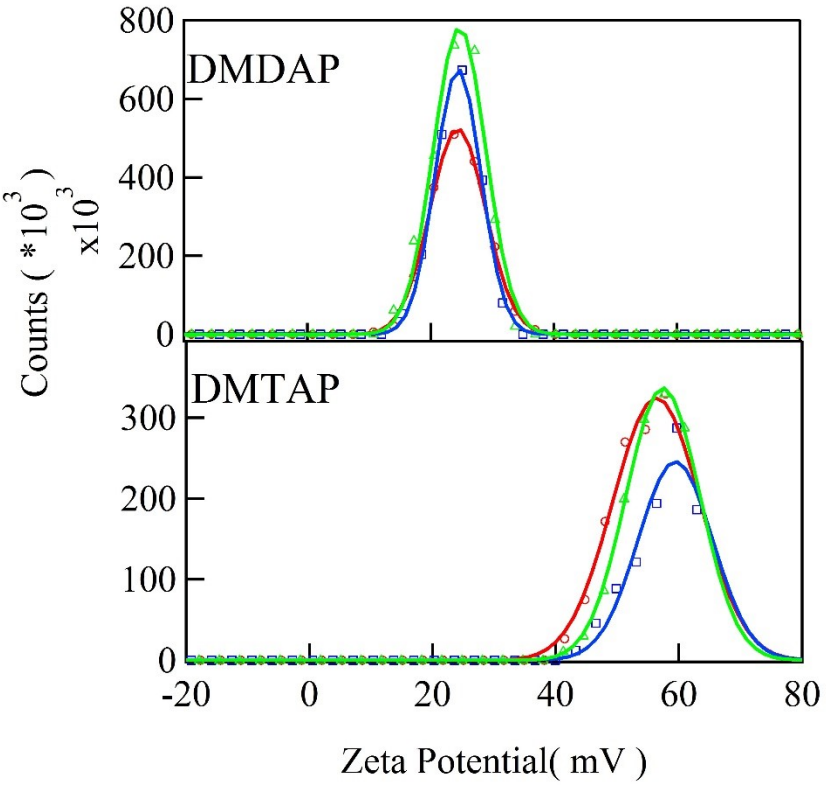

Figure S3 The potential-dependent counts of DMTAP liposome and DMDAP liposome. The solid lines are the Guass fitting curve of the liposome counts from each zeta potential measurement.

Table S1. The fitting parameters of zeta potential data.

Lipid	**DMTAP**	**DMDAP**
ζ_0	56.4	24.4
width	10.0	6.40
ζ_0	59.4	24.5
width	8.54	5.25
ζ_0	57.4	24.7
width	8.47	6.01
Average ζ_0	57.7 ± 2.2	24.5 ± 0.2

S4. Calculation of surface charge density and surface potential

The surface charge density can be calculated based on the mean molecular area of the lipid molecules at 32 mN/m and the head group ionization ratio of each lipid monolayer. It should be noted that in this calculation, only the charge of the outer leaflet of lipid bilayers is considered. The charge/ionization ratio of –tri-methyl-ammonium groups (DMTAP, DMEPC), and –di-methyl-ammonium groups (DMDAP) were set as +0.85, +0.5, and +0.4, respectively.[1]

$$\Psi_0 = \frac{2k_BT}{e}\sinh^{-1}\left(\frac{\sigma_{sum}}{\sqrt{8000k_BTN_AC\varepsilon_0\varepsilon_r}}\right) \quad \backslash^* MERGEFORMAT\ (S1)$$

where σ_{sum} is the summation of surface charge density, k_B, N_A are the Boltzmann constant and the Avogadro constant, ε_r and ε_0 relative dielectric constant, dielectric constant in vacuum, C is the molar electrolyte constant.[2-6]

Table S2. Estimated surface charge density and surface potential of lipid membranes

	Lipid	DMTAP	DMDAP
Monolayer	Mean molecular area (Å^2)	69.5	38.4
Bilayer before interaction	Surface Charge Density (C/M^2)	0.196	0.166
	Surface Potential (mV)	+288	+246
	Liposome Zeta Potential (mV) *	57.7 ± 2.2	24.5 ± 0.2

S5. SFG spectra of unconjugated AS1411 molecules

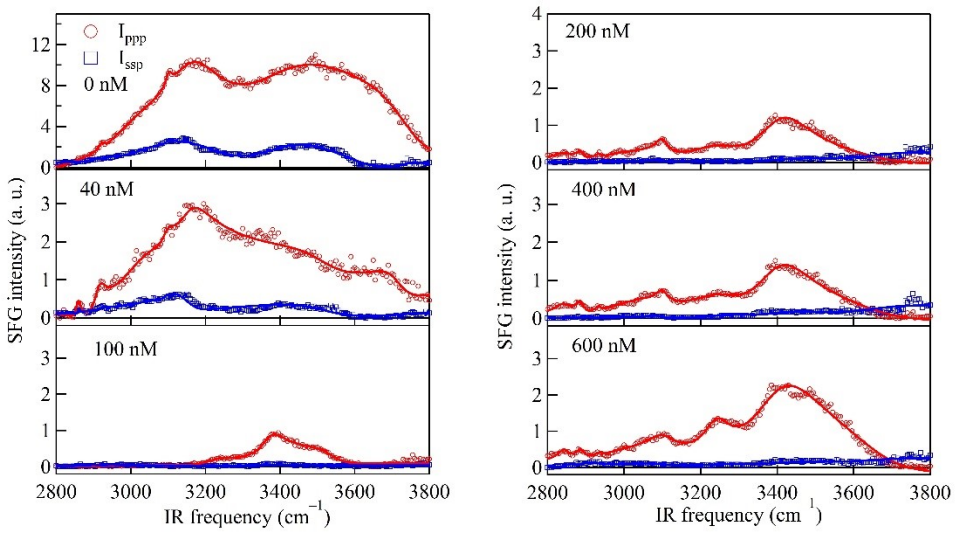

Figure S4 SFG spectra of unconjugated AS1411 molecules interacting with DMTAP lipid bilayers in the wavenumber range of 2800−3800 cm^{-1}.

S6. SFG spectra of the lipid bilayer in D_2O

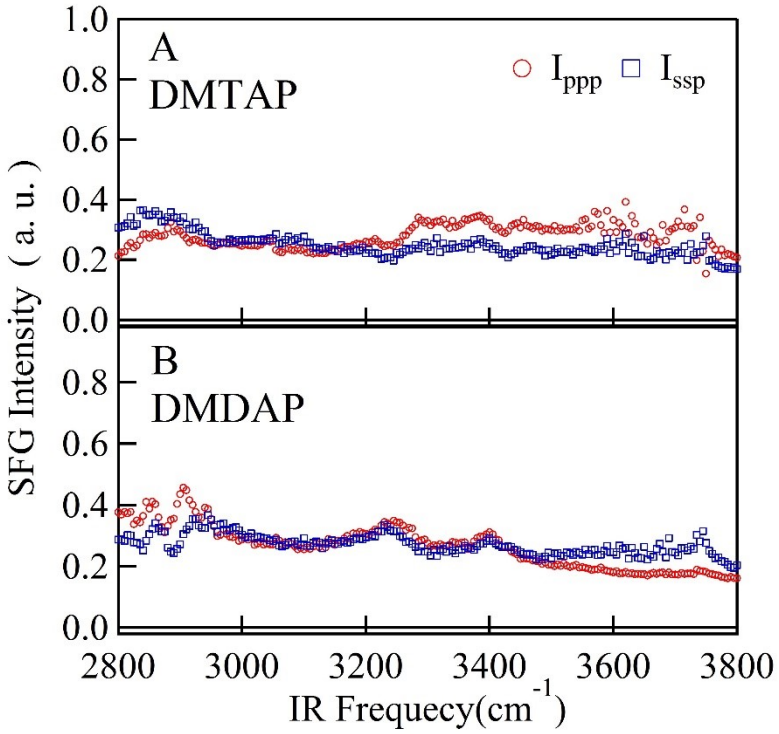

Figure S5 SFG spectra of (A) DMTAP and (B) DMDAP lipid bilayers in D_2O solution.

S7. Fitting of SFG−VS Signals

As described in detail elsewhere, the intensity of the SFG light is proportional to the square of the sample's second-order nonlinear susceptibility ($\chi_{eff}^{(2)}$), and the intensity of the two input fields $I_1(\omega_{vis})$ and $I_2(\omega_{IR})$, see eq. (S1). $\chi_{eff}^{(2)}$ vanishes when the structure of contributing molecules/medium has an inversion of symmetry.[2-6]

$$I(\omega_{SFG}) \propto \left|\chi_{eff}^{(2)}\right|^2 I_1(\omega_{vis}) I_2(\omega_{IR}) \qquad \backslash^* \text{ MERGEFORMAT (S2)}$$

where $\omega_{SFG} = \omega_{IR} + \omega_{vis}$. As the IR beam frequency is tuned over a vibrational resonance of surface/interface molecules, the effective surface nonlinear susceptibility can be greatly enhanced. By assuming the frequency dependence of $\chi_{eff}^{(2)}$ at the charged surface in the ionic solution can be described is described by: [2-5]

$$\chi_{eff}^{(2)}(\omega_{IR}) = \chi_{NR}^{(2)} + \chi_s^{(2)} + \chi_{EDL}^{(2)} = \chi_{NR}^{(2)} + N_s \chi_s^{(2)} + C_B \chi_B^{(3)} \frac{k}{k + i\Delta k_z} \Psi_0 \qquad \backslash^*$$

$$\text{MERGEFORMAT (S3)}$$

$$1/k = \left(8\pi L_B c_{salt}\right)^{-\frac{1}{2}};\ \frac{0.304}{\sqrt{c_{salt}}} nm \qquad \backslash^* \text{ MERGEFORMAT (S4)}$$

where $\chi_{NR}^{(2)}$ $\chi_s^{(2)}$ and $\chi_{EDL}^{(2)}$ are the non-resonant response, the response of molecules on the surface, and the response of molecules in electric double layer respectively. If we assume the molecules on the surface and the molecules in the electrical double layer have the same vibrational resonance.

The fitting parameters ($1/k$, $1/\Delta k_z$, Ψ_0) in different salt concentrations are listed in Table S3. The plot of the SFG signal vs. the IR input frequency shows a polarization-dependent vibrational spectrum of the molecules at the surface or interface. A_υ, ω_υ, and Γ_υ can be extracted by fitting the spectrum using Eq.S5.

$$\chi_{eff}^{(2)}(\omega_{IR}) = \chi_{NR}^{(2)} + \sum_{\upsilon} \frac{A_s^{(2)} + \Psi_0 A_B^{(3)} \frac{k}{k + i\Delta k_z}}{\omega_{IR} - \omega_\upsilon + i\Gamma_\upsilon}$$

$$= \chi_{NR}^{(2)} + \sum_{\upsilon} \frac{A_s^{(2)}(\omega_{IR} - \omega_\upsilon) + \Psi_0[A_B^{(3)}(\omega_{IR} - \omega_\upsilon)F_1 - A_B^{(3)}\Gamma_\upsilon F_2]}{(\omega_{IR} - \omega_\upsilon)^2 + {\Gamma_\upsilon}^2} + \frac{A_s^{(2)}\Gamma_\upsilon + \Psi_0[A_B^{(3)}(\omega_{IR} - \omega_\upsilon)F_2 + A_B^{(3)}\Gamma_\upsilon F_1]}{(\omega_{IR} - \omega_\upsilon)^2 + {\Gamma_\upsilon}^2}$$

* MERGEFORMAT (S5)

$$F_1 = \frac{k^2}{k^2 + {\Delta k_z}^2}$$ * MERGEFORMAT (S6)

$$F_2 = \frac{k\Delta k_z}{k^2 + {\Delta k_z}^2}$$ * MERGEFORMAT (S7)

where ω_υ, and Γ_υ are the resonant frequency, and damping coefficient of the vibrational mode(ν), respectively. $A_s^{(2)}, A_B^{(3)}$ are the amplitudes of the second-order susceptibilities of the surface and third-order susceptibilities of the EDL.

Table S3. The fitting parameters for $\chi_{EDL}^{(2)}$.

Concentration Mol/L	$1/k$ nm	$1/\Delta k_z$ nm	F_1	F_2
0.001	96.1	43	0.1667	0.3727

S8. The fitting parameters of AS1411 molecules

Table S4. The fitting parameters of AS1411 molecules

Molecules				Assignments
DMTAP AS−A	DMTAP AS−C	DMDAP AS−A	DMDAP AS−C	
1370	1382	1370	1370	C_2' −endo/syn−dG
1398	1400	1398	1398	CH_2 bending
1450	1450	1450	1450	CH_3 bending
1484	1475	1483	1482	dG−N_5 ring stretching
1538	1533	1539	1539	dG−N_7 ring stretching
1570	1569	1569	1569	dG or dT ring

				stretching
1611	1611	1610	1610	dG–NH_2 bending
1662	1662	1659	1665	dT in-phase C_4=O/C_5=C_6 stretching
1710	1715	1709	1713	dG C_6=O & C_8=C_9 stretching
N/A	N/A	N/A	2847	CH_2- symmetric stretching
N/A	N/A	N/A	2877	CH_3- symmetric stretching
N/A	3087	3070	3072	CH stretching in dG and dT
3171	3145	3114	3118	NH stretching in dG and dT
3265	3264	3255	3256	NH_2-Fermi
3397	3396	3389	3392	NH_2 symmetric stretching
N/A	3479	3480	3485	NH_2 anti-symmetric stretching

S9. The orientation and Susceptibilities of molecular groups

The molecular orientation information can be obtained by relating SFG susceptibility tensor elements $\chi_{ijk}(i,j,k=x,y,z)$ in the laboratory frame to the SFG molecular hyperpolarizability tensor elements $\beta_{lmn}(l,m,n=a,b,c)$ in the molecular frame via the Euler transformation.[6, 7] The Euler transformation used here follows the z-x-y convention, which has a matrix in the following formula.

$$\chi^{(2)}_{ijk,q} = \sum_{l,m,n} N_s \left\langle R_{il} R_{jm} R_{kn} \right\rangle \beta_{lmn,q} \qquad \backslash^* \textit{MERGEFORMAT (S8)}$$

$$R_{il,jm,kn} = \begin{pmatrix} -\sin(\varphi)\cos(\theta)\sin(\psi)+\cos(\varphi)\cos(\psi) & -\sin(\varphi)\cos(\theta)\cos(\psi)-\cos(\varphi)\sin(\psi) & \sin(\varphi)\sin(\theta) \\ \cos(\varphi)\cos(\theta)\sin(\psi)+\sin(\varphi)\cos(\psi) & \cos(\varphi)\cos(\theta)\cos(\psi)-\sin(\varphi)\sin(\psi) & -\cos(\varphi)\sin(\theta) \\ \sin(\theta)\sin(\psi) & \sin(\theta)\cos(\psi) & \cos(\theta) \end{pmatrix} \backslash^* \textit{MERGEFORMAT (S}$$

The components of the $\chi^{(2)}_{eff}$ of the ssp, and ppp polarization combinations are given in susceptibilities in the lab coordinate system which is defined as the z-axis is along the surface normal and the x-axis is in the incident plane.[8-11]

$$\chi^{(2)}_{eff,ssp} = L_{yy}(\omega_{SF})L_{yy}(\omega_{Vis})L_{zz}(\omega_{IR})\sin\beta_{IR}\chi^{(2)}_{yyz} \qquad \backslash^* \textit{MERGEFORMAT (S10)}$$

$$\begin{aligned}\chi^{(2)}_{eff,ppp} = &-L_{xx}(\omega_{SF})L_{xx}(\omega_{Vis})L_{zz}(\omega_{IR})\cos\beta_{SF}\cos\beta_{Vis}\sin\beta_{IR}\chi^{(2)}_{xxz}\\ &-L_{xx}(\omega_{SF})L_{zz}(\omega_{Vis})L_{xx}(\omega_{IR})\cos\beta_{SF}\sin\beta_{Vis}\cos\beta_{IR}\chi^{(2)}_{xzx}\\ &+L_{zz}(\omega_{SF})L_{xx}(\omega_{Vis})L_{xx}(\omega_{IR})\sin\beta_{SF}\cos\beta_{Vis}\cos\beta_{IR}\chi^{(2)}_{zxx}\\ &+L_{zz}(\omega_{SF})L_{zz}(\omega_{Vis})L_{zz}(\omega_{IR})\sin\beta_{SF}\sin\beta_{Vis}\sin\beta_{IR}\chi^{(2)}_{zzz}\end{aligned} \qquad \backslash^* \textit{MERGEFORMAT (S11)}$$

where β_{SF}, β_{Vis}, and β_{IR} are the angles between the surface normal and the sum frequency beam, the input visible beam, and the input IR beam, respectively. L_{ii} (i = x, y or z) denotes the Fresnel coefficients.

For lipid monolayers at CaF_2/air interface, Eq. S10 and Eq. S11 are then given by:

$$\chi^{(2)}_{\mathrm{eff,ssp}} = 1.229\chi^{(2)}_{\mathrm{yyz}} \qquad \backslash^* \textit{MERGEFORMAT (S12)}$$

$$\chi^{(2)}_{\mathrm{eff,ppp}} = -0.127\chi^{(2)}_{\mathrm{xxz}} - 0.120\chi^{(2)}_{\mathrm{xzx}} + 0.115\chi^{(2)}_{\mathrm{zxx}} + 1.374\chi^{(2)}_{\mathrm{zzz}} \qquad \backslash^* \textit{MERGEFORMAT (S13)}$$

Because $\chi^{(2)}_{xxz}$ equals to $\chi^{(2)}_{yyz}$ for C_∞ symmetry, the $\chi^{(2)}_{xxz}$ and $\chi^{(2)}_{zzz}$ susceptibility components are the main contributors to the ssp and ppp signals, respectively. With an azimuthal symmetry of the molecules at the interface, the dependence of $\chi^{(2)}_{xxz}$ and $\chi^{(2)}_{zzz}$ susceptibility components on the molecular hyperpolarizability can be described by the following equations. [8-11]

A mode:

$$\chi^{(2),A}_{xxz} = \chi^{(2),A}_{yyz} = N_s\beta_{ccc}G(\theta) = N_s\beta_{ccc}\frac{1}{2}\left([r+1]\langle\cos\theta\rangle + [r-1]\langle\cos^3\theta\rangle\right) \qquad \backslash^* \textit{MERGEFORMAT (S14)}$$

$$\chi^{(2),A}_{zzz} = N_s\beta_{ccc}G(\theta) = N_s\beta_{ccc}[r\langle\cos\theta\rangle + (1-r)\langle\cos^3\theta\rangle] \qquad \backslash^* \textit{MERGEFORMAT (S15)}$$

where $r = \frac{\beta_{aac}}{\beta_{ccc}} = \frac{\beta_{bbc}}{\beta_{ccc}} = \frac{\alpha_{aa}^{(2)}}{\alpha_{cc}^{(2)}} = \frac{\alpha_{bb}^{(2)}}{\alpha_{cc}^{(2)}}$.

For the lipid bilayers and AS1411 molecules at CaF_2/water interface, the Fresnel coefficient constants are then given by:

$$\chi_{\mathrm{eff,ssp}}^{(2)} = 1.319\chi_{\mathrm{yyz}}^{(2)} \qquad \text{* MERGEFORMAT (S16)}$$

$$\chi_{\mathrm{eff,ppp}}^{(2)} = -0.137\chi_{\mathrm{xxz}}^{(2)} - 0.110\chi_{\mathrm{xzx}}^{(2)} + 0.105\chi_{\mathrm{zxx}}^{(2)} + 1.184\chi_{\mathrm{zzz}}^{(2)} \qquad \text{* MERGEFORMAT (S17)}$$

Because $\chi_{xxz}^{(2)}$ equals to $\chi_{yyz}^{(2)}$ for C_∞ symmetry, the $\chi_{xxz}^{(2)}$ and $\chi_{zzz}^{(2)}$ susceptibility components are the main contributors to the ssp and ppp signals, respectively. With an azimuthal symmetry of the molecules at the interface, the dependence of $\chi_{xxz}^{(2)}$ and $\chi_{zzz}^{(2)}$ susceptibility components on the molecular hyperpolarizability can be described by the following equations. [8-11]

A_1 mode:

$$\begin{aligned}\chi_{xxz}^{(2),A1} = \chi_{yyz}^{(2),A1} = {} & \frac{1}{2}N_s\beta_{ccc}[\langle\cos^2\psi\rangle r_a + \langle\sin^2\psi\rangle r_b + 1]\langle\cos\theta\rangle \\ & + \frac{1}{2}N_s\beta_{ccc}[\langle\sin^2\psi\rangle r_a + \langle\cos^2\psi\rangle r_b - 1]\langle\cos^3\theta\rangle\end{aligned} \qquad \text{* MERGEFORMAT (S18)}$$

$$\begin{aligned}\chi_{zzz}^{(2),A1} = {} & N_s\beta_{ccc}[\langle\sin^2\psi\rangle r_a + \langle\cos^2\psi\rangle r_b]\langle\cos\theta\rangle \\ & - N_s\beta_{ccc}[\langle\sin^2\psi\rangle r_a + \langle\cos^2\psi\rangle r_b - 1]\langle\cos^3\theta\rangle\end{aligned} \qquad \text{* MERGEFORMAT (S19)}$$

where ψ is the twisting angle of the nucleotide base groups.

For the nucleotide groups which can be freely rotated, the Eq. S18 and Eq. S19 can be simplified into:

$$\chi_{xxz}^{(2),A1} = \chi_{yyz}^{(2),A1} = N_s\beta_{ccc}G(\theta) = N_s\beta_{ccc}\frac{1}{4}\left([r_a + r_b + 2]\langle\cos\theta\rangle + [r_a + r_b - 2]\langle\cos^3\theta\rangle\right) \qquad \text{* MERGEFORMAT (S2}$$

$$\chi_{zzz}^{(2),A1} = N_s\beta_{ccc}G(\theta) = N_s\beta_{ccc}\frac{1}{2}\left([r_a + r_b]\langle\cos\theta\rangle - [r_a + r_b - 2]\langle\cos^3\theta\rangle\right) \qquad \text{* MERGEFORMAT (S21)}$$

where

$$r_a = \frac{\beta_{aac}}{\beta_{ccc}} = \frac{\alpha_{aa}^{(2)}}{\alpha_{cc}^{(2)}} \qquad \backslash * \ MERGEFORMAT\ (S22)$$

$$r_b = \frac{\beta_{bbc}}{\beta_{ccc}} = \frac{\alpha_{bb}^{(2)}}{\alpha_{cc}^{(2)}} \qquad \backslash * \ MERGEFORMAT\ (S23)$$

S9.1 CH_3 symmetric stretching mode

By setting the r value for the CH_3-SS mode as 3.4, the deduced tilt angle related function of susceptibilities $G(\theta)_{ppp}$, $G(\theta)_{ssp}$, and susceptibility ratio $R = \chi^{(2)}_{\mathrm{ppp,CH_3\text{-}ss}} / \chi^{(2)}_{\mathrm{ssp,CH_3\text{-}ss}} = G(\theta)_{ppp} / G(\theta)_{ssp}$ can be plotted as a function of the tilt angle.

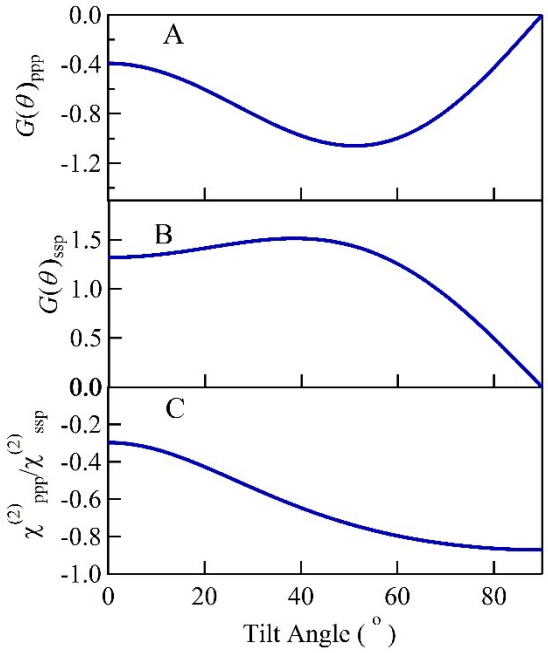

Figure S6 Simulated tilt angle related function of susceptibilities (A) $G(\theta)_{ppp}$, (B) $G(\theta)_{ssp}$, and (C) susceptibility ratio $R = \frac{\chi^{(2)}_{ppp}}{\chi^{(2)}_{ssp}} = \frac{G(\theta)_{ppp}}{G(\theta)_{ssp}}$ of CH_3 symmetric stretching mode.

S9.2 Thymine C_4=O & C_5=C_6 in phase stretching mode

The Raman tensors of thymidine groups at 1665 cm^{-1} have been reported in previous literature (C1 coordinates, $r_a = \frac{\alpha_{aa}^{(2)}}{\alpha_{cc}^{(2)}} = 4.31$, $r_b = \frac{\alpha_{bb}^{(2)}}{\alpha_{cc}^{(2)}} = 0.25$).[12, 13] The molecular coordinate is determined by taking the plane of thymine aromatic ring as bc plane and taking the $\vec{\mu}_{C_4=O}$ vector as c-axis. The IR dipole moment at the wavenumber of C_4=O & C_5=C_6 in-phase mode either can be the same as the vector of C_4=O bond or can be calculated using the vibration displacements of each atom ($\frac{\partial x}{\partial Q}, \frac{\partial y}{\partial Q}, \frac{\partial z}{\partial Q}$) listed in the Guassian output file (*.out or *.gjy). [12, 13]

$$\frac{\partial \vec{\mu}_Q}{\partial Q} = \sum_n M_n \left(\frac{\partial x}{\partial Q}\frac{\partial \mu_n}{\partial x}\vec{x} + \frac{\partial y}{\partial Q}\frac{\partial \mu_n}{\partial y}\vec{y} + \frac{\partial z}{\partial Q}\frac{\partial \mu_n}{\partial z}\vec{z} \right) \quad \backslash^* \textit{MERGEFORMAT (S24)}$$

Where M_n is the relative mass of each atom, $\frac{\partial \mu_n}{\partial x}$, $\frac{\partial \mu_n}{\partial y}$ and $\frac{\partial \mu_n}{\partial z}$ are the dipole derivatives of each atom listed at the end of the Guassian output file. It should also be noted that the guanine residues also have contributions to SFG intensities around 1665 cm^{-1}, which may affect the accuracy of the fitting results of 1665 cm^{-1} (C_4=O & C=C in phase stretching of thymine groups) peak.

Table S5. Derivatives of Raman tensors and IR transition dipoles of C_4=O & C_5=C_6 in phase stretching mode at 1665 cm^{-1}.

Vibrational mode	$\frac{\partial \alpha_{\text{Raman}}}{\partial Q}$	$\frac{\partial \mu_{\text{IR}}}{\partial Q}$
Data from Ref. 13	$\begin{vmatrix} 0.232 & 0 & 0 \\ 0 & 0.058 & 0 \\ 0 & 0 & 1 \end{vmatrix}$	$\begin{vmatrix} 0 \\ 0 \\ 1 \end{vmatrix}$
Calculated Results*	$\begin{vmatrix} 0.329 & 0.137 & -0.283 \\ 0.137 & 0.127 & -0.142 \\ -0.283 & -0.142 & 0.834 \end{vmatrix}$	$\begin{vmatrix} 0 \\ 0 \\ 1 \end{vmatrix}$

*The derivatives of IR dipole of Thymidine groups were calculated by Guassian 09 using

Hartree-Fork method with 3-21G+** basis.[14]

The deduced susceptibilities $\chi^{(2)}_{ppp}$, $\chi^{(2)}_{ssp}$, and susceptibility ratio $\chi^{(2)}_{\mathrm{ppp,thymine}} / \chi^{(2)}_{\mathrm{ssp,thymine}}$ can also be plotted as a function of the tilt angle.

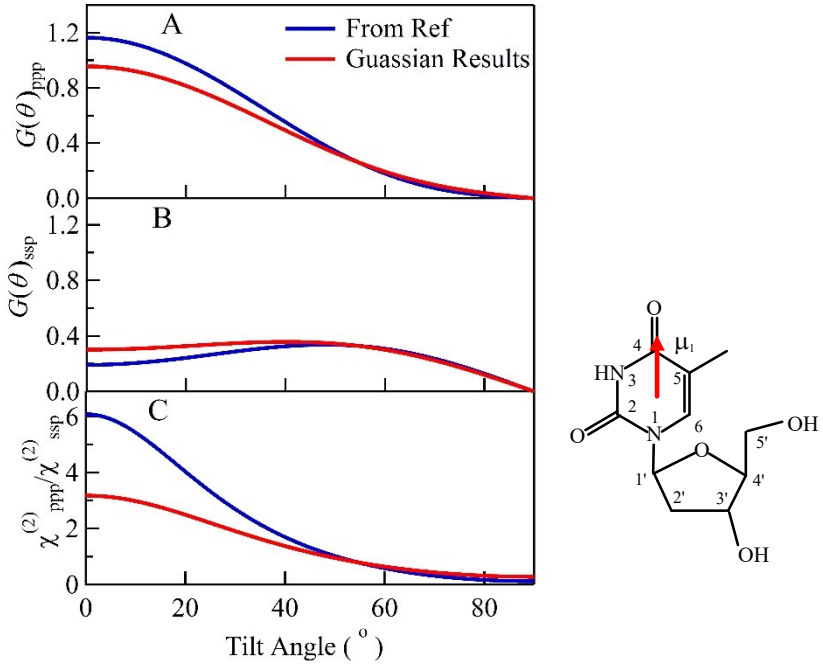

Figure S7 Simulated tilt angle related function of susceptibilities (A) $G(\theta)_{ppp}$, (B) $G(\theta)_{ssp}$, and (C) susceptibility ratio $R = \frac{\chi^{(2)}_{ppp}}{\chi^{(2)}_{ssp}} = \frac{G(\theta)_{ppp}}{G(\theta)_{ssp}}$ of C_4=O & C_5=C_6 in phase stretching mode of thymine group.

S9.3 Guanine dG−N_5 ring stretching mode at ~1485 cm^{-1}.

The Raman tensors of guanine residue at ~1485 cm^{-1} were reported in previous literature.[15, 16] The IR dipole of guanine residue (G7K, most stable) was calculated by Guassian09 using Hartree-Fork 3-21G+** method. [14] The molecular coordinate is determined by taking the plane of guanine aromatic ring as YZ plane, the $\vec{V}_{N_7-N_5}$ vector as Y-axis, and the $\vec{V}_{C_6=O}$ vector as Z-axis. The IR dipole moment at the wavenumber of 1485cm^{-1} was calculated using the vibration displacements of each atom listed in *.out file.

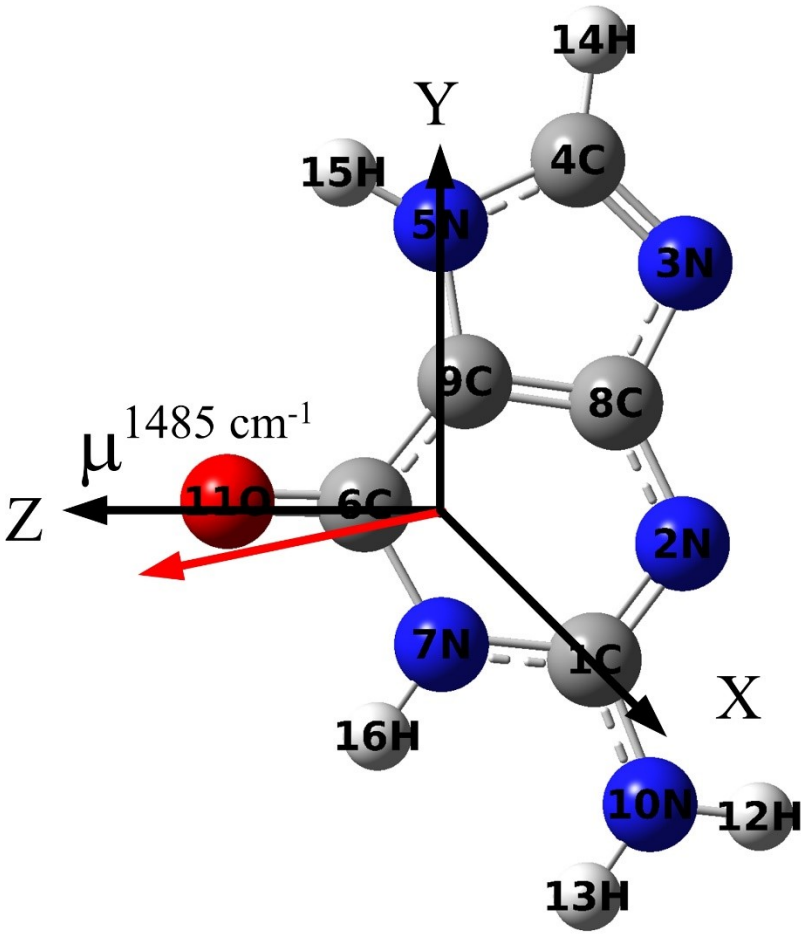

Figure S8. The IR dipole of Guanine base residue which calculated by Guassian09.

The Raman tensors and IR dipoles of quadruplex structures were calculated based on the NMR results and molecular coordinates of oligonucleotide molecules. The PDB IDs for C_{12}TG14 and C_{12}Oxy28 are 148D and 201D respectively (**DOI:**10.2210/pdb148d/pdb and **DOI:**10.2210/pdb201d/pdb) . The detailed calculation methods can be found in recent reviews. [10, 11]

Table S6. Raman tensors and IR dipoles of guanine residue at 1485 cm^{-1}(dG–N_5 ring stretching).

Structure	α_{Raman}	μ_{IR}

Data from Ref. 13	$\begin{vmatrix} 0.023 & 0 & 0 \\ 0 & 1 & 0 \\ 0 & 0 & 1 \end{vmatrix}$	$\begin{vmatrix} 0 \\ 0 \\ 1 \end{vmatrix}$
Calculated Results*	$\begin{vmatrix} 0.149 & 0 & 0 \\ 0 & 1 & 0 \\ 0 & 0 & 1 \end{vmatrix}$	$\begin{vmatrix} 0.107 \\ 0.328 \\ 0.938 \end{vmatrix}$

According to the calculation results, the deduced tilt angle related function of susceptibilities ($^{G(\theta)_{ppp}}$,$^{G(\theta)_{ssp}}$) and susceptibility ratio $R = \chi^{(2)}_{ppp}/\chi^{(2)}_{ssp}$ of dG–N_5 ring stretching of the guanine groups are plotted as a function of the tilt angle.

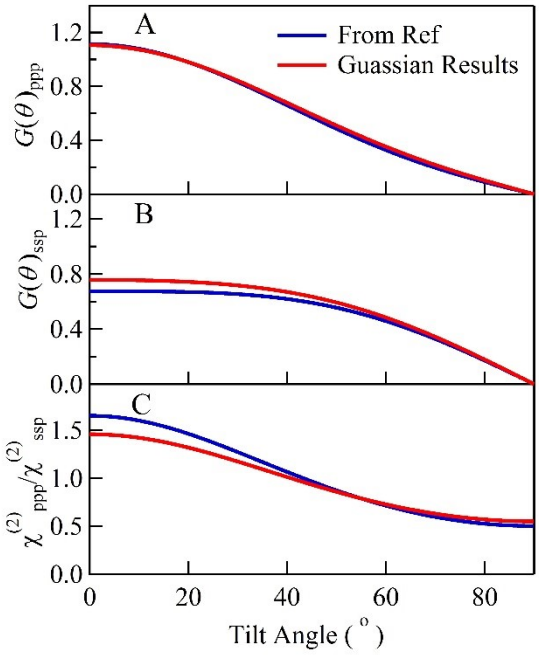

Figure S9 Simulated tilt angle related function of susceptibilities (A) $^{G(\theta)_{ppp}}$, (B) $^{G(\theta)_{ssp}}$, and (C) susceptibility ratio $R = \frac{\chi^{(2)}_{ppp}}{\chi^{(2)}_{ssp}} = \frac{G(\theta)_{ppp}}{G(\theta)_{ssp}}$ of dG–N_5 ring stretching of guanine groups.

S10. **Time dependence of the calculated SFG** susceptibility **ratios**

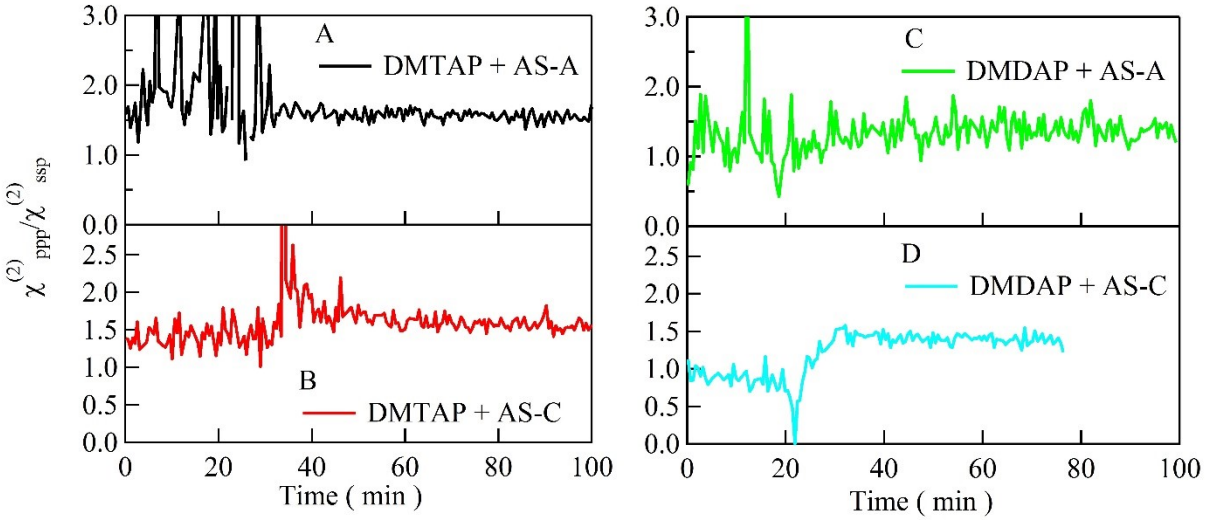

Figure S10 The time dependence of the calculated SFG susceptibility ratios $R_{1665} = \sqrt{I_{ppp} / I_{ssp}}$ (1665 cm^{-1}) during the adsorption of conjugated AS1411 molecules on cationic lipid membranes. (A) DMTAP + AS−A; (B) DMTAP + AS−C; (C) DMDAP + AS−A; (D) DMDAP + AS−C.

Reference

1. Roberts, J. D.; Clement, R. A.; Drysdale, J. J., The Electrical Effect of the Trimethylammonium [−$N(CH_3)_3\oplus$] Group. *J. Am. Chem. Soc.* **1951,** *73*, 2181-2183.

2. Gonella, G.; Lütgebaucks, C.; de Beer, A. G. F.; Roke, S., Second Harmonic and Sum-Frequency Generation from Aqueous Interfaces Is Modulated by Interference. *J. Phys. Chem. C* **2016**, *120*, 9165-9173.

3. Wang, H. F., Sum frequency generation vibrational spectroscopy (SFG−VS) for complex molecular surfaces and interfaces: Spectral lineshape measurement and analysis plus some controversial issues. *Prog. Surf. Sci.* **2016**, *91*, 155-182.

4. Ohno, P. E.; Wang, H. F.; Geiger, F. M., Second-order spectral lineshapes from charged interfaces. *Nat. Comm.* **2017,** *8*, 1032.

5. Ohno, P. E.; Wang, H. F.; Paesani, F.; Skinner, J. L.; Geiger, F. M., Second-Order Vibrational Lineshapes from the Air/Water Interface. *J. Phys. Chem. A* **2018,** *122*, 4457-4464.

6. Y. R. Shen, The Principles of Nonlinear Optics, 1st ed; John Wiley& Sons: New York, 1984.

7. Moad, A. J.; Simpson, G. J. A Unified Treatment of Selection Rules and Symmetry Relations

for Sum-Frequency and Second Harmonic Spectroscopies. *J. Phys. Chem. B* **2004**, *108*, 3548-3562.

8. Chen, X.; Wang, J.; Boughton, A. P.; Kristalyn, C. B.; Chen, Z. Multiple Orientation of Melittin inside a Single Lipid Bilayer Determined by Combined Vibrational Spectroscopic Studies. *J. Am. Chem. Soc.* **2007**, *129*, 1420-1427.

9. Wang, J.; Lee, S. H.; Chen Z. Quantifying the Ordering of Adsorbed Proteins in Situ. *J. Phys. Chem. B* **2008**, *112*, 2281-2290.

10. Nguyen, K. T.; Le Clair, S. V.; Ye, S.; Chen, Z. Orientation Determination of Protein Helical Secondary Structures Using Linear and Nonlinear Vibrational Spectroscopy. *J. Phys. Chem. B* **2009**, *113*, 12169-12180.

11. Lee, S.; Wang, J.; Krimm, S.; Chen, Z. Quantifying the Ordering of Adsorbed Proteins In Situ. *J. Phys. Chem. A* **2006**, *110*, 7035-7044.

12. Thomas, G. J., Jr.; Benevides, J. M.; Overman, S. A.; Ueda, T.; Ushizawa, K.; Saitoh, M.; Tsuboi, M., Polarized Raman spectra of oriented fibers of A DNA and B DNA: anisotropic and isotropic local Raman tensors of base and backbone vibrations. *Biophys. J.* **1995,** *68*, 1073-1088.

13. Benevides, J. M.; Overman, S. A.; Thomas, G. J., Raman, polarized Raman and ultraviolet resonance Raman spectroscopy of nucleic acids and their complexes. *J. Raman Spectrosc.* **2005,** *36*, 279-299.

14. Gaussian 09, Revision D.01, Frisch, M. J.; Trucks, G. W.; Schlegel, H. B.; Scuseria, G. E.; Robb, M. A.; Cheeseman, J. R.; Scalmani, G.; Barone, V.; Mennucci, B.; Petersson, G. A.; Nakatsuji, H.; Caricato, M.; Li, X.; Hratchian, H. P.; Izmaylov, A. F.; Bloino, J.; Zheng, G.; Sonnenberg, J. L.; Hada, M.; Ehara, M.; Toyota, K.; Fukuda, R.; Hasegawa, J.; Ishida, M.; Nakajima, T.; Honda, Y.; Kitao, O.; Nakai, H.; Vreven, T.; Montgomery, J. A., Jr.; Peralta, J. E.; Ogliaro, F.; Bearpark, M.; Heyd, J. J.; Brothers, E.; Kudin, K. N.; Staroverov, V. N.; Kobayashi, R.; Normand, J.; Raghavachari, K.; Rendell, A.; Burant, J. C.; Iyengar, S. S.; Tomasi, J.; Cossi, M.; Rega, N.; Millam, M. J.; Klene, M.; Knox, J. E.; Cross, J. B.; Bakken, V.; Adamo, C.; Jaramillo, J.; Gomperts, R.; Stratmann, R. E.; Yazyev, O.; Austin, A. J.; Cammi, R.; Pomelli, C.; Ochterski, J. W.; Martin, R. L.; Morokuma, K.; Zakrzewski, V. G.; Voth, G. A.; Salvador, P.; Dannenberg, J. J.; Dapprich, S.; Daniels, A. D.; Farkas, Ö.; Foresman, J. B.; Ortiz, J. V.; Cioslowski, J.; Fox, D. J. Gaussian, Inc., Wallingford CT, **2009**.

15. Miura, T.; Thomas, G. J., Structural Polymorphism of Telomere DNA: Interquadruplex and Duplex-Quadruplex Conversions Probed by Raman Spectroscopy. *Biochemistry* **2002,** *33*, 7848-7856.